A BIAXIAL SHEARING APPARATUS TO STUDY THE MICROMECHANICS OF SAND USING A 2-D ANALOGUE PHOTOELASTIC MATERIAL

R.G. Wan, Department of Civil Engineering, University of Calgary, Canada.
M. Al-Mamun, Department of Civil Engineering, University of Calgary, Canada.
K. Sawada, Department of Civil Engineering, Gifu University, Japan.

ABSTRACT
The role of microstructure (fabric) on the strength of sands is experimentally verified through the use a 2-D analogue granular material. A special biaxial shearing apparatus was constructed for testing an assembly of photoelastic polyurethane polygonal disks along imposed strain paths. The stress-induced birefringence property of the disks provides a unique feature that enables us to observe optically microstructural information such as the force transmission network through contact points. Thus, the macroscopic behavioural properties of a granular material such as dilatancy can be related to microscopic information like particle interconnectivity and fabric. The paper discusses the biaxial shearing apparatus, testing scheme, and some test results pertaining to the analysis (mechanical and optical) of a series of strain probing tests with focus to the roles played by dilatancy and fabric in the failure of granular soils. These provide deep insights and important information that can used to construct a constitutive model for sand with embedded microstructural information.

RÉSUMÉ
Le rôle de la microstructure des sables sur leur résistance est vérifié en faisant appel à des expériences sur un matériau analogique bidimensionnel. Nous imposons un chemin de déformation à un ensemble de disques (polygones) dans un appareil de cisaillement biaxial que nous avons construit dans cette étude. Le fait que les disques sont faits d'un matériau photoélastique permet la visualisation des structures microstructurelles par le biais d'un réseau de forces transmises aux points de contacts. Les propriétés macroscopiques du matériau granulaire, telle que la dilatance, peuvent donc être reliées a l'interconnectivité des grains, càd la microstructure. Nous décrivons l'appareil de cisaillement, le programme des expériences, et quelques résultats obtenus concernant le comportement du matériau granulaire sur des chemins de déformations. Nous évoquons l'importance de la dilatance et la microstructure dans les schémas de rupture. Les résultats peuvent aussi déboucher sur l'élaboration des lois de comportement des sables avec des informations microstructurelles.

1. INTRODUCTION

Granular soils such as sands are composed of discrete particles connected through a number of contact points within a complex microstructure that responds to externally applied loads. These loads are transmitted through the interparticle contacts which develop into a network of force chains. These dictate the shear strength, dilatancy and stability of the bulk material. For instance, the liquefaction behaviour of sands hinges upon the material's background property such as dilatancy which is closely intertwined with fabric and force chain development. In the limiting case, a dense sand with the right fabric may even succumb to unstable behaviour such as liquefaction in undrained conditions. Hence, the role of fabric on the strength characteristics of a sand is an important issue in geomechanics, and its experimental investigation is of interest.

The fundamental problem is to characterize the kinematics and statics of individual sand grains in a granular mass, and thereafter relate them to known macroscopic properties such as shear strength and dilatancy. In this context, analogue materials such as glass balls and rods (Rowe, 1962), wooden rollers (Calvetti et al., 1997), and coins (François et al., 2002) have been used to indirectly study the physics of sand deformation. An assembly of photoelastic disks has also been used for a long time (Drescher et al., 1972; Konishi, 1978; Oda et al., 1982) in order to optically visualize force chain network development, and hence fabric changes. In addition to behaving as an idealized discrete medium, each photoelastic disk in the assembly has a high optical sensitivity so as to produce visible colour fringes under applied stress and strain. Hence, not only the overall stress strain response, but also the microscopic force transmission mechanisms can be observed.

In this paper we will describe a biaxial shearing apparatus that was designed and constructed to study both the micro- and macro-mechanical responses of an idealized photoelastic disk assembly. The results obtained from 'proportional strain path testing' under forced compression and dilation will be reported in the context of internal microstructural evolution and its relation to material strength. One of the ramifications of this study is that material instability can occur in paths other than the conventional isochoric (undrained) condition. Also, it is demonstrated that the material strength is generally not bounded by the undrained and drained conditions that are routinely used as reference in geotechnical analysis.

2. ANALOGUE MATERIAL

The material that was used is a photoelastic polyurethane (PSM4) material that is available in sheets of various thicknesses. The physical and optical properties of the

material are as follows: material fringe value F=0.15 kPa/fringe/m, elastic modulus E=4 MPa, and Poisson's ratio υ=0.5. The material fringe value is a parameter that links optical information to applied stresses as a function of the light wavelength used. A sheet of thickness 9.375 mm (3/8 inch) was chosen from which pentagonal shaped disks were cut using a band saw. The pentagons are regular and inscribed into a circle of 7 mm in diameter. Circular disks of 5 and 7 mm were also used. These were prepared by casting the material into moulds of various sizes to produce the desired disk diameter (Micromeasurements, Inc.). Pictures of the disks are shown in Figure 1.

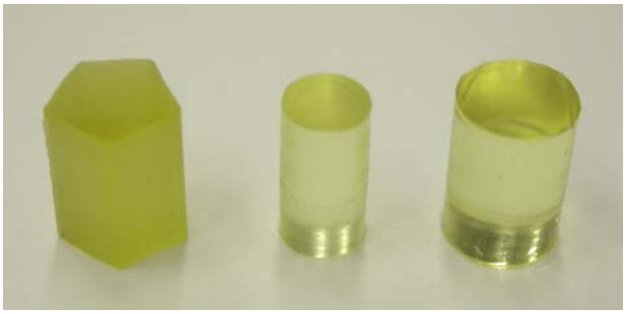

Figure 1. Photoelastic disks of different shapes and diameters

3. APPARATUS

3.1 Biaxial shearing apparatus

Figure 2 shows the schematics of the apparatus developed in this study. It consists of a loading chamber that is bounded by four separate loading beams. The height of these beams was made equal to that of the disks. Each of the loading beams is free to move and has a pair of small bearings at one end. These bearings can slide very smoothly over the nearby beam (normal to it) so as to reduce friction. The loading beams were made wide enough (25 mm) so that they do not tilt, and thereby will distribute the loads uniformly on the specimen to be tested. A load is applied to each beam through a 'guide-way' that has two ends (see Figure 2). The one end near the loading beam was made as wide as possible to make sure that load applied will spread uniformly enough so that the chance of any eccentricity developing will be minimal. The guide-way has three equally spaced bearings to transmit the applied load to the loading beam without any friction loss. Another advantage of the bearings is that they permit the loading beams to move laterally as well. The other end of the guide-way also has a small beam, which connects with a load cell that measures load applied on the specimen along that direction. The overall mechanism of the apparatus is such that all four loading beams can independently move with minimal friction loss so that the loading chamber can collapse into any size.

High precision step motors (Model: 3.3-A083AB-HT23-8-1-/4,Ultramotions LLC.) were used to move the linear actuators that push the loading beam through the guide-way at different speeds (displacement rates). The step motors permit the application of any rate of deformation onto the specimen along any direction.

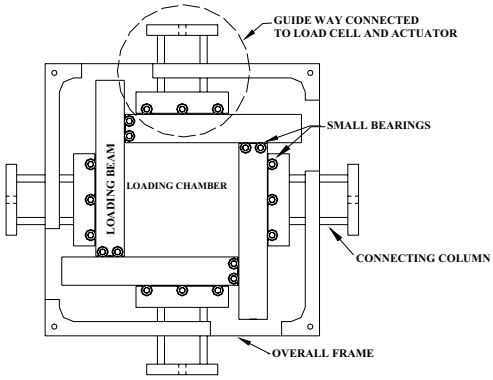

Figure 2. A schematic view of the biaxial shearing apparatus showing its different components

The LVDT's (Linear Variable Differential Transducers) were connected to measure the displacement of the loading beams in each direction. Therefore, four sets of actuators, LVDT's, load cells, and step motors constitute four independent arms. The four load cells and four LVDT's were connected to a data acquisition software (LabTech Notebook Pro 10.1) installed in a PC. The motors and actuators were connected to an individual 'programmable step motor driver' (Model: 3540i, Applied Motion Products, Inc.). These four drivers were linked to a central 'hub', which was finally connected to another PC. A motion control software 'SiNet Hub Programmer' (v.1.79, Applied Motion products, Inc.) was used to operate the actuators through these drivers. This software has a user-friendly graphical user interface and a set of commands, so that actuators can be programmed in any combination and at any speed. A schematic view of the arrangement is shown in Figure 3.

In the above discussed arrangement, the load can also be controlled indirectly by changing the displacement in order to maintain any desired load. A top plate made of plexiglas was used to cover the loading chamber. The outside dimensions of the apparatus are 240 mm by 240 mm with a variable loading chamber area that can accommodate a specimen area ranging from a maximum size of 105 mm×105 mm to a minimum one of 90 mm×90 mm. The biaxial shearing apparatus was placed horizontally to exclude the effect of the gravity with respect to the loading directions.

3.2 Verification of accuracy

Several tests were performed at the beginning to check the accuracy of the measured load from the four load cells in comparison to the actual loads on the specimen. Possible friction loss emanate from (a) the guide-way mechanism, (b) the junction at two perpendicular loading beams, and (c) the degree of accuracy within which the force is measured at the boundary of the specimen.

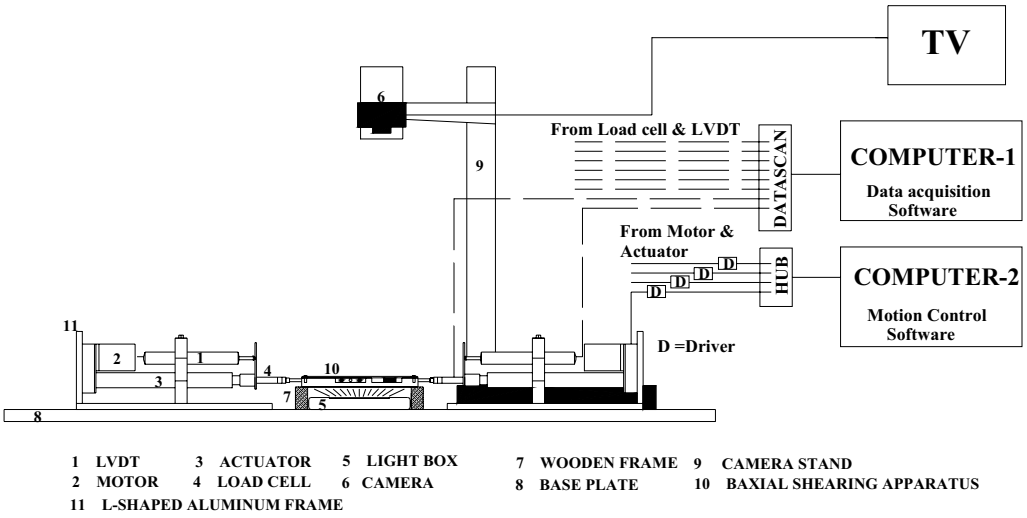

Figure 3: Schematics of the side view of the test arrangement showing the biaxial apparatus, loading arms, camera stand with all other peripheral components such as computers, TV monitor, and data acquisition setup

It was first decided to verify that all applied forces transmit to the specimen and no force losses due to the movement of the body of the apparatus or any other components. A simple test was conducted to check this. As shown in Figure 4, three load cells were placed in line where two of them were connected to the guide-way and one of them was placed inside the loading chamber. The load was applied through one guide-way, and the transmitted load in the inside load cell and the reaction on the load cell at other side were measured. Observed responses were plotted in Figure 4(b) which shows a good agreement of all three load readings. Therefore, the loss of force in the guide-way mechanism is very small, if at all negligible.

At the corner points of the loading chamber where two loading beams touch each other, any possible friction loss was taken care of by using a pair of bearings, see Figure 2. As such, there was no possibility of any force concentration at these corners at any stage of deformation of the specimen. Furthermore, a thin piece of plastic sheet was pasted on the inside edge of the loading beams which provide a very smooth surface and reduce frictional loss.

For completeness, several tests were conducted to check the force transmission along two principal directions so that it can be confidently assumed that the forces measured in each of the load cells mounted on the four loading beams reflect the ones actually acting on the specimen boundaries. The specimen was loaded isotropically by applying the same rate of displacement from all four sides and measuring the corresponding load cell readings. The load-deflection responses in all four directions were virtually the same with a maximum deviation of 3 N in the high load range, i.e. 100 N. This indicates that the forces along two principal directions are the same (isotropy is achieved). Also, most importantly, the forces on the two sides of the specimen in each principal direction are the same. This means that the force transmission through the specimen along each direction is uniform. If the readings on two load cells aligned in one direction were different, this would mean unaccounted frictional losses in the loading system. In the analysis, we take the average of the pair of load cell readings along each of the principal directions as: $F_1=(F_2+F_4)/2$ and $F_2=(F_1+F_3)/2$. Here F_1, F_2, F_3, and F_4 are the readings of the four load cells. This averaging minimizes the small deviation in the load cell readings if there is any, and also justifies the use of four independent load cells instead of only two along two principal directions. In the case of two load cells along two principal directions, uniform load transmission at other ends cannot be verified.

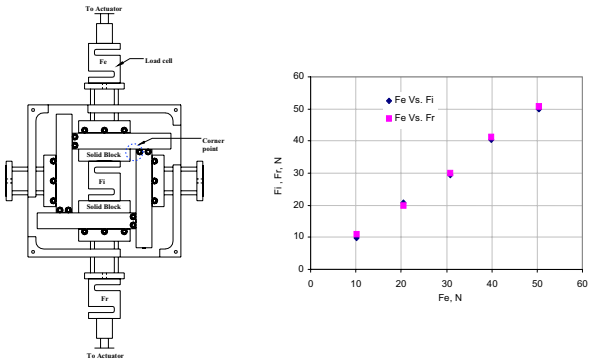

(a) (b)

Figure 4. Verification of in-line transfer of loading and frictional loss

3.3 Arrangement for photoelastic observations

The biaxial shearing apparatus was placed in a circular polariscope arrangement to permit the viewing of the fringes that developed in the specimen during loading. The apparatus was placed between a pair of circular polarizers as shown in the Figure 5.

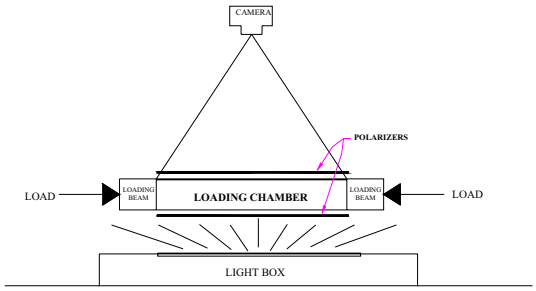

Figure 5. Schematic view of the photoelastic arrangement including a circular polariscope for viewing the fringes in the specimen

A flat light box was placed beneath the apparatus so that light can pass through the specimen, and fringes become visible from the top (see Figure 3). A digital camera (Model: Nikon Coolpix4500), mounted on a stand, was focused from the top in order to capture pictures. A TV monitor (32.5 cm) was used as external video output so that the photoelastic fringes on the specimen can be viewed clearly on a wide screen which facilitates the image capturing process (see Figure 3).

4. DETAILS OF THE EXPERIMENTS

4.1 Straining combinations

The biaxial shearing apparatus can be used to apply a wide range of deformation rate (from 0.0159 mm/s to 1.0 mm/s) in the specimen along two principal directions through the four loading arms. As the loading arms can move back and forth at any predetermined displacement rate, the specimen can be subjected to both forced compactive and dilative strains, as well as a combination of both along two principal directions. For a given major principal direction, these can be broadly categorized into the following four groups:

1. Forced compression along both major and minor principal directions (CC).
2. Forced extension along both major and minor principal directions (EE).
3. Forced compression along major and forced extension along minor principal directions (CE).
4. Forced extension along major and forced compression along minor principal directions (EC).

For CC and EE tests, the specimens were forced to pure compression and dilation states respectively, whereas for cases of CE and EC, it depends on the relative magnitudes of the rate of compression and extension applied from two principal directions (D_1 and D_2). Figure 6 shows location of four straining combinations (CC, EE, CE, EC) in the D_1 versus D_2 space for better understanding. For example, any point in CC quadrant is a result of a combination of D_1 and D_2 such that both of them are compressive.

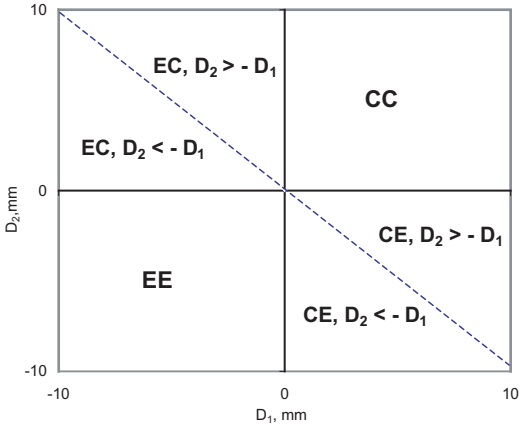

Figure 6. The location of the straining combinations in D_1 versus D_2 space

Standard tests such as conventional drained triaxial test (here biaxial) and one-dimensional consolidation tests can be simulated by controlling strain rates. For biaxial drained tests (deviatoric stress increasing keeping radial stress constant), D_1 is increased (so that deviatoric force increases) and D_2 is adjusted such that force along this direction ($\Delta F=0$) remains almost the same. Again, for 1-D consolidation tests, D_1 changes while $D_2=0$ or vice versa. Stress control probing type of tests can also be conducted by changing D_1 and D_2 within very small value so that load increment along that direction can be controlled precisely.

4.2 Specimen preparation

The disks were placed in the loading chamber manually one by one resting on the bottom plate, until completely full. As the biaxial shearing apparatus was placed horizontally, the stacking process leading to either a dense or a loose packing was easy. The top plate was kept slightly above the specimen so that no friction developed. Friction between the specimen and the bottom plate was also negligible as both of the surfaces of the disk and the bottom plexiglass were very smooth. The photoelastic disks were soft and hence very sensitive to the application of a very small amount of force. During the preparation of the specimen, care was taken so that all the disks remain stress-free and merely touch each other. The disks were arranged in a random fashion to form dense packing.

The initial specimen area was kept to be square ($L_1=L_2=$ 94.6 mm), containing 220 pentagons. In order to confine the specimen isotropically, it was compressed from all four sides at a certain displacement rate (0.05 mm/s). It is

important to note that, the apparatus is strain controlled and it was not very precise to achieve any predefined amount of force. Hence, we have to permit some degree of variation in the stresses observed on all four sides, especially when we worked in the small load range such as 5 N or 10 N. However, in most of the cases, the loads applied were in the order of 20 N or higher, and the previously mentioned force variation remained less than 4%. In the experiments where it was intended to reproduce the same fabric and void ratio for a series of tests, we used the same number of pentagons occupying the same area in each tests.

5. TEST RESULTS

5.1 Proportional strain paths

The proportional strain paths are due to an imposed constant deformation rate ϑ defined as the rate of volumetric strain ($d\varepsilon_v$) over that of shear strain ($d\gamma$) on the specimen. As such, a special case of isochoric (area preserving) deformations refers to the condition of ϑ=0. Also, imposed dilation and compaction correspond to ϑ<0 and ϑ>0 respectively. Strain path controlled experimental studies are scarce in the literature, with the exception of the work reported by Chu et. al. (1992) that probes sand behaviour along proportional strain paths with reference to strain softening, localization, as well as material stability. From a practical viewpoint, Vaid and Sivathayalan (2000) have also investigated strain path tests by controlling the drainage conditions in the test specimen since water flowing into or out of it would cause either dilation or contraction. The rationale of such tests is that under real field situations, soils deform in a partially drained condition. On the other hand, there have also been various numerical explorations of material behaviour in proportional strain paths, see Darve & Laouafa (2002), and Wan & Guo (2004).

5.2 Proportional strain path in biaxial stress state

In view of testing the material along proportional strain paths, both axial and lateral displacement rates ($\dot{D}_1$ & $\dot{D}_3$ respectively) are applied in a ratio defined as $\vartheta^* = (\dot{D}_1 + \dot{D}_3)/(\dot{D}_1 - \dot{D}_3)$. Hence, forced dilatant and contractant strain paths refer to negative and positive ϑ^* values respectively, whereas the isochoric deformation condition is given by $\vartheta^* = 0$. The axial and lateral forces arising from applied displacements are also measured as f_1 and f_3 respectively.

A relatively dense packing of pentagons is achieved by carefully placing the particles one by one in a consistent manner in a given pattern so that the initial packing of the specimen is repeatable. Then, the specimen is consolidated at a targeted confining pressure of 20 N, and thereafter forced to deform along various strain paths of ϑ^* values. The resulting force response path is analyzed by plotting the deviatoric force $f_d = (f_1 - f_2)/2$ against the mean force $f_m = (f_1 + f_2)/2$.

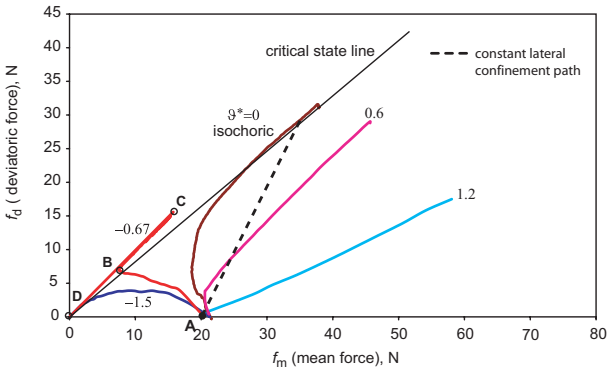

Figure 7. Force path response for various constant rates of dilation and compaction

Figure 7 shows the force response paths resulting from shearing along some selected strain paths that range from imposed compaction to dilation. One immediate observation is that material response is not bounded by the ones given in the constant lateral confinement (drained test) and the isochoric (undrained test) conditions. In other words, the densely packed granular material may well display unstable behaviour if it were taken along a dilatant path (e.g. $\vartheta^* = -0.67$ & -1.5), while it would display stable hardening behaviour when forced to compact (e.g. $\vartheta^* = 0.6$ & 1.2).

It is of interest to examine the force response path pertaining to an imposed dilation rate of $\vartheta^* = -0.67$ which displays an initial hardening phase (BC) followed by a snap back phase (CD), whereby the material suffers an abrupt collapse. To further examine this phenomenon, the evolutions of axial (f_1), lateral (f_2) and mean (f_m) forces are shown in Figure 8. There is a general increase in axial forces during the hardening phase despite a drop in lateral forces. At failure, the drop in lateral forces exacerbates.

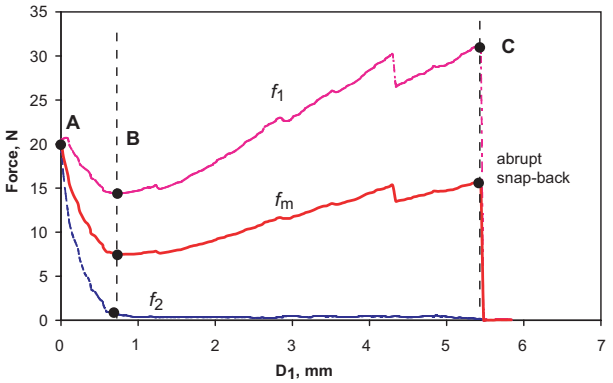

Figure 8. Force component evolutions: dilatant path ϑ^*= -0.67

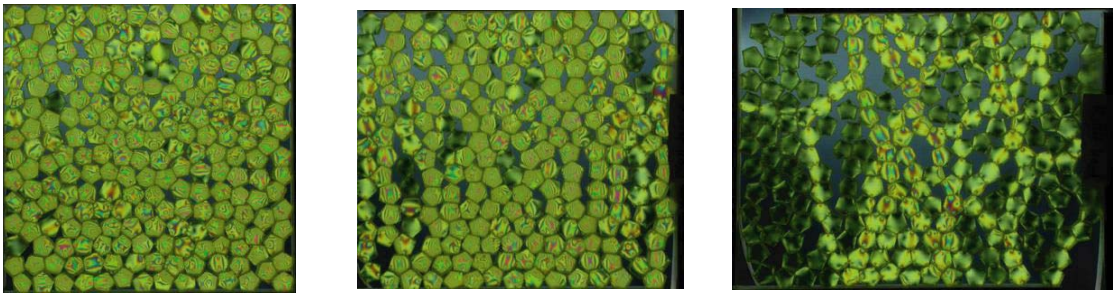

initially (A) turning point (B) snap-back point (C)

Figure 9. Evolution of microstructure at different key points along dilatant path ϑ^*= -0.67

Figure 9 gives the contact force chain and associated structure at key points A, B and C on the force response curve plotted in Figure 7. The fringe patterns indeed indicate the formation of contact force chains along path A-B while both axial and lateral loads are being reduced. Between B and C, additional force chains develop in the axial direction as the axial load picks up. At the same time, in order to sustain the imposed deformations as prescribed by ϑ^*, the lateral load has to decrease so as to allow the required dilation. The force chains ultimately buckle at point C, giving an abrupt snap back in load response. At this point, the material response is very unstable with failure associated to a complete loss of load bearing capacity due to the disaggregation of particles. This is germane to a percolation threshold at which all the contact forces (effective stresses) vanish.

5.3 Friction and dilation angles under forced dilation

A few more dilatant paths (ϑ^* <0) complementing those given in Figure 7 are plotted in Figure 10 with the isochoric case (ϑ^* = 0) as lower bound.

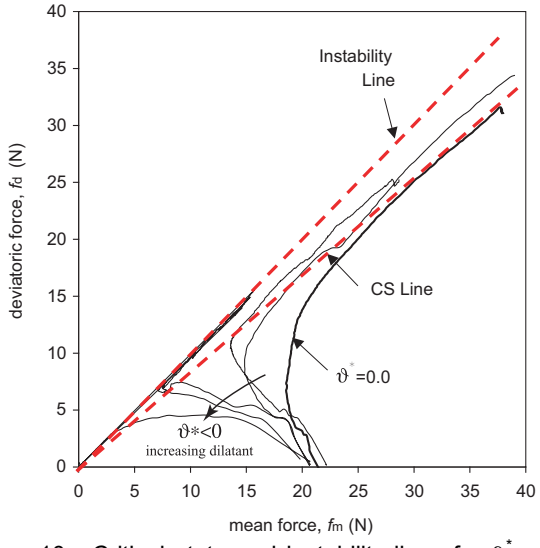

Figure 10. Critical state and instability lines for ϑ^* paths under forced dilation

All force response paths show an asymptotic behaviour that can be characterized by some 'failure' line whose inclination is defined as α, an angle that can be related to some apparent friction angle φ. The failure line that coincides with the isochoric force response path is necessarily the constant volume (Critical State, CS) line by definition. As the forced dilation increases, the force response paths cross the CS line and ultimately lead to failure lines with increasing angles α. In fact, there is a series of failure lines with the CS line being the lower bound and a so-called 'instability' line as the upper bound. In general, the angle α refers to a compounded friction angle that includes the effect of dilation. Therefore, the instability line refers to the limiting dilation rates that the specimen can experience before it succumbs to instability failure.

The angle α can be related to the internal friction angle φ of a granular material using Mohr-Coulomb failure criterion, i.e. $\sin\varphi = (\sigma_1 - \sigma_3)/(\sigma_1 + \sigma_3)$, where σ_1 and σ_3 are the major and minor principal stresses. Converting forces into stresses through the use of some cross-sectional area, and assuming that forces f_1 and f_2 give rise to major and minor principal stresses, it turns out that $\sin\varphi = \tan\alpha$. Turning to the CS line, a measured value of $\alpha = 39.8^0$ gives an angle of friction at constant volume φ_{cv} of 56.4^0, which is quite high in comparison to sand for which $\varphi_{cv} \cong 32^0$-34^0. For objective comparison purposes, it is to be mentioned that Geng et al. (2001) measured a `true' friction angle, $\varphi_\mu \cong 44^0$, measured from the friction developed between two pentagonal disks formed of the same photoelastic material used in this study. Given that φ_{cv} is generally larger than φ_μ, it is concluded that our measured φ_{cv} is reasonable. Konishi et al. (1978) measured $\varphi_\mu \cong 52^0$ for oval disks of a different type of photoelastic material. Furthermore, it is also worth mentioning that the friction angles measured in this study are derived from plane strain conditions, and generally higher than those determined in axi-symmetric stress and strain conditions. In soil mechanics, it is known that the difference in friction angle between plane strain and axi-symmetric stress and strain conditions can be as high as 8^0 (Cornforth, 1964).

Recalling the definition of the imposed dilation rate $\vartheta^* = (\dot{D}_1 + \dot{D}_2)/(\dot{D}_1 - \dot{D}_2)$, we can obtain a dilatancy angle ψ based on kinematical conditions and considering the Mohr circle of strains (Hansen, 1958), i.e.

$$\sin\psi = (\dot{D}_1 + \dot{D}_2)/(\dot{D}_1 - \dot{D}_2) = \vartheta^* \qquad [1]$$

Since for each test, the enforced dilation rate ϑ^* (hence dilation angle ψ) is known, a relationship between the apparent friction angle, φ_p , as derived from α and dilation angle can be established. Table 1 shows the measured as well as transformed data.

Table 1. List of dilation angles observed from static and kinematic analyses.

ϑ^*	α (deg)	φ_p (deg)	$\varphi_p - \varphi_{cv}$	$\sin^{-1}(\vartheta^*)$
0	39.8	56.4(=φ_{cv})	0	0
-0.2	41.5	62.1	5.7	11.5
-0.33	42.1	64.5	8.1	19.3
-0.60	43.18	69.8	13.4	36.8
-0.67	44	74.9	18.5	42
-0.75	45	90	33.6	48.6

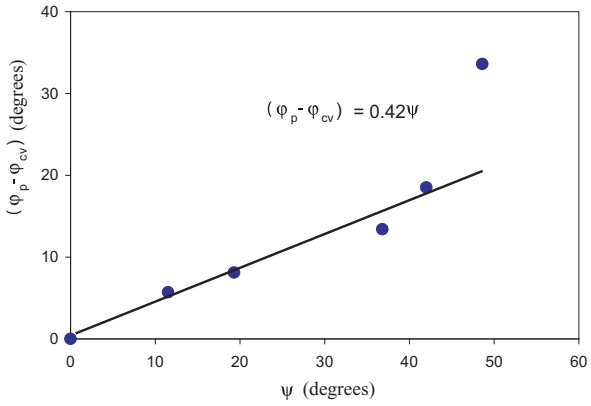

Figure 11. Relationship between peak, constant volume and dilatancy angles as derived from both kinematic and static analyses

From the above Figure 11, we arrive at the following relationship, i.e.

$$\varphi_p = \varphi_{cv} + 0.4\psi \qquad [2]$$

It is noted that the last point corresponding to the limiting value α lies on the instability line, and has been discarded in the analysis. Only data points which are within the stable material behaviour region have been retained. It is interesting to note that the relationship established in Equation 2 is similar to the well known relationship developed by Bolton (1986) which gives

$$\varphi_p = \varphi_{cv} + 0.8\psi \qquad [3]$$

derived from experimental data on sand.

6. CONCLUSIONS

The experimental work reported in this paper elucidates the underlying failure mechanisms at the microstructural level that describe both the shearing and instability behaviours of granular soils. The studies on assemblies of photoelastic disks reveal the formation of a network of force chains, the stability of which controls the failure behaviour of the bulk material. Biaxial shearing test results on the shearing of an assembly of photoelastic disks along different strain paths with various degrees of forced dilation and compaction illustrate the whole spectrum of material behaviour. Translating these results into soil mechanics, it is found that both the failure strength and instability behaviour of a sand are not bounded by the undrained (isochroric) and drained triaxial testing conditions that are routinely used as baseline. Interestingly, it is found that a dense granular material can succumb to an instability like flow behaviour if taken along a strain path corresponding to a critical dilation rate. By contrast, the same dense sand shows a stable behaviour under strain paths with isochoric deformation, i.e. undrained conditions. This suggests that the liquefaction behaviour of sands hinges upon the material's background property such as dilatancy and the interplay with dilatancy and fabric structure. It is also interesting to note that the experimental results support the numerical simulations reported by Wan & Guo (2004) on sand behaviour with respect to fabric and dilatancy issues.

ACKNOWLEDGEMENT

Funding provided by the Natural Science and Engineering Council of Canada, and the Alberta Energy Research Institute is gratefully acknowledged.

REFERENCES

Bolton, M.D. 1986. The strength and dilatancy of sands. Geotechnique, Vol. 35, No. 2, pp. 99-112.

Calvetti, F., Combe, G., and Lanier, J., 1997. Experimental micromechanical analysis of a 2D granular material: relation between structure evolution and loading path. Mechanics of Cohesive-Frictional Materials, Vol. 2, pp. 121-163.

Chu, J., Lo, S-C. R., and Lee, I. K., 1992. Strain-softening behaviour of granular soil in strain-path testing. J. Geotech. Eng. ASCE, Vol. 118, No. 2, pp. 191-208.

Cornforth, D.H, 1964. Some experiments on the influence of strain conditions on the strength of sand. Geotechnique, Vol 14, No. 2, pp. 143-167.

Darve, F., and Laouafa, F., 2002. Constitutive equations and instabilities of granular materials. Modeling and Simulation in Science, Engineering and Technology, eds: Gaiuf R., C., Vito N. G., and Pasquale Giovine, Birkhauser, pp. 3-43.

Drescher, A., and Josselin de Jong G., 1972. Photoelastic verification of mechanical model for the flow of a granular material. J. Mech. Phys. Solids, Vol. 20, pp. 337-351.

François, B., Lacombe, F., and Herrmann, H. J., 2002. Finite width of shear zones. Physical Review E. Vol. 75, 031311.

Hansen, B. 1958. Lines ruptures regarded as narrow rupture zone, basic equation based on kinematic conditions. Proceedings of the Conference of Earth Pressure Problems, Brussels, Belgium, pp. 39-51.

Geng, J., Howell, D., Longhi, E., Behringer, R.P., Reydellet, G., Vanel, L.,Clement, E., and Luding, S., 2001. Footprints in sand: The response of a granular material to local perturbations. Physical Review Letters, Vol. 87, No3, 035506-1.

Konishi, J., 1978. Microscopic model studies on the mechanical behavior of granular materials. In: S.C. Cowin and M. Satake, eds., Proc. U.S.-Japan seminar on Continuum-Mechanical and Statistical Approaches in the Mechanics of Granular Materials, Gakujutsu bunken Fukyukai, Tokyo, pp. 27-45.

Oda, M., 1982. Fabric tensor for discontinuous geological materials. Soils & Foundations, Vol. 22, No. 4, pp. 96-108.

Rowe, P.W. 1962. The stress-dilatancy relation for static equilibrium of an assembly of particles in contact. Proc. of Royal Soc. A 269, pp. 500-527.

Vaid, Y. P., and Saivathayalan, S., 2000. Fundamental factors affecting liquefaction susceptibility of sands, Can Geotech. J., Vol. 37, pp. 592-606.

Wan, R. and Guo, P., 2004. Stress dilatancy and fabric dependencies on sand behavior. Journal of Engineering Mechanics, Journal of Engineering Mechanics, ASCE, Vol. 130, No. 6, pp. 635-645.